MLP-GAN for Brain Vessel Image Segmentation

Bin Xie[1], Hao Tang[2], Bin Duan[1], Dawen Cai[3], Yan Yan[1]
[1]Department of Computer Science, Illinois Institute of Technology, Chicago, IL, USA
[2]Computer Vision Lab, ETH, Zurich, Switzerland
[3]Department of Cell and Developmental Biology, University of Michigan, Ann Arbor, MI, USA
{bxie9, bduan2}@hawk.iit.edu, hao.tang@vision.ee.ethz.ch, dwcai@umich.edu, yyan34@iit.edu

***Abstract*—Brain vessel image segmentation can be used as a promising biomarker for better prevention and treatment of different diseases. One successful approach is to consider the segmentation as an image-to-image translation task and perform a conditional Generative Adversarial Network (cGAN) to learn a transformation between two distributions. In this paper, we present a novel multi-view approach, MLP-GAN, which splits a 3D volumetric brain vessel image into three different dimensional 2D images (*i.e.*, sagittal, coronal, axial) and then feed them into three different 2D cGANs. The proposed MLP-GAN not only alleviates the memory issue which exists in the original 3D neural networks but also retains 3D spatial information. Specifically, we utilize U-Net as the backbone for our generator and redesign the pattern of skip connection integrated with the MLP-Mixer [1] which has attracted lots of attention recently. Our model obtains the ability to capture cross-patch information to learn global information with the MLP-Mixer. Extensive experiments are performed on the public brain vessel dataset [2] that show our MLP-GAN outperforms other state-of-the-art methods. We release our code at https://github.com/bxie9/MLP-GAN.**

I. Introduction

Medical image analysis has achieved numerous and remarkable progress with deep learning [3], [4], [5] for the past few years. For example, brain vessel image segmentation [2] can be used as a promising biomarker for disease diagnosis and prevention via 3D MRI analysis which is quite meaningful to human health studies. However, brain vessel image segmentation is a complicated task due to the interweaving nature and different thicknesses of brain vessels. The image segmentation problem actually can be considered as an image-to-image translation task that transforms original images into segmentation masks, which can be solved by conditional Generative Adversarial Network (cGAN). Therefore, in this paper, we utilize cGAN to solve the brain vessel image segmentation task.

However, it is quite challenging to build a large 3D medical dataset due to the difficulty of acquisition and annotation. Thus, we used a synthetic brain vessel dataset [2] that is accurately annotated. Meanwhile, 3D-based deep learning architectures in literature have numerous parameters, which mean significant computation resources are needed. To address these problems, one straightforward approach is to simply use 2D-based deep neural networks by slicing 3D volumetric images into a sequence of 2D plane images along only one dimension. However, this simple strategy will cause the inevitable loss of useful 3D spatial information. Therefore, in this paper, we propose a novel multi-view approach that splits 3D volumetric images into a sequence of 2D plane images in three different planes (*i.e.,* coronal, sagittal, axial), as shown in Figure 1, for the same arranged indexes to be fed into three different 2D-based cGANs. In this way, we not only alleviate the memory issue which exists in the original 3D neural networks but also retain 3D spatial information.

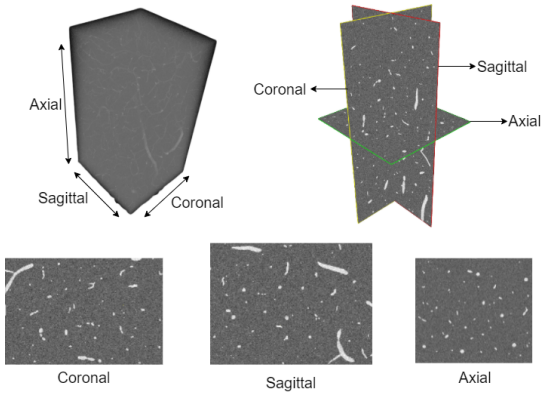

Fig. 1. Brain vessel image. The shape of the original brain vessel data is (325, 304, 600). The three spatial dimensions are namely coronal, sagittal, and axial, respectively.

Specifically, we utilize the U-Net [3] as the backbone for our generator network. Although the skip connections in the original U-Net combine shallow, low-level, and fine-grained feature maps to deep, semantic, and coarse-grained feature maps, a simple concatenation cannot maximize their benefits. Recently, MLP-Mixer [1] has been proposed and obtained lots of attention due to cross-patch and cross-channel communication. Therefore, we redesign our model with the MLP-Mixer as MLP-Mixer enhanced generator. We design different patterns of skip connection by MLP-Mixer to eliminate the semantic gap among different feature maps.

To summarize, we have the following contributions:

- We propose a novel MLP-GAN for the brain vessel image segmentation task. We involve the recent MLP-Mixer to learn global information to improve the performance.
- To alleviate the memory issue and retain 3D spatial information, we split 3D volumetric images into a sequence of 2D plane images by three different planes and then feed them into three different 2D MLP-based GANs.
- We redesign the patterns of skip connection. Each layer in the decoder can learn more semantic information since we utilize the MLP-Mixer layer to mix deeper level layers'

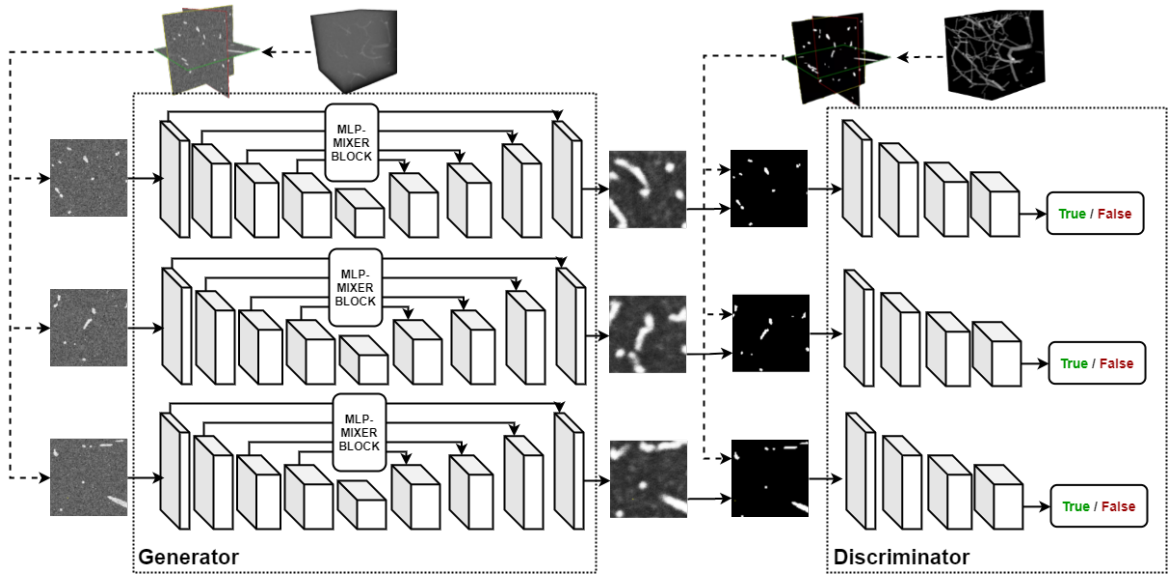

Fig. 2. The overview of our proposed MLP-GAN network. The overview of our proposed MLP-GAN network. Firstly, a cube image (256, 256, 256) is sliced into a sequence of $256 \times (256, 256)$ three plane images with the same index ranged [0, 255]. Every patch of three plane images will be fed into three individual 2D U-Net-based networks, respectively. Then the generator generates three fake images, which are fed into the discriminator with three ground truth segmentation maps. In order to maximize the benefit of skip connections, we replace and redesign all concatenations using MLP-Mixer, since MLP-Mixer can achieve patch-wise communication by *channel-mixing* and *token-mixing* MLPs.

and current level layer's information from the encoder to learn overall information.

- We conduct extensive experiments on a public brain vessels dataset [2]. Both qualitative and quantitative results demonstrate that the proposed MLP-GAN achieves new state-of-the-art results for the task.

II. Related work

A. GANs for Medical Images Segmentation

Generative Adversarial Networks (GANs) [6] have been widely and successfully used for image-to-image translation tasks [7], [8], [9], [10], which translate one domain of images to another domain by learning how to transform the distributions of the two classes. For instance, Isola et al. [7] utilized a conditional GAN to replace the standard noise vector with a source image as input to learn the mapping from input images to target images. Recently, GANs also achieved state-of-the-art results in the medical image segmentation task [11], [12], [13], [14], [15], [16], [17], [18]. For instance, Mondal et al. [18] introduced a novel method based on GANs to train a segmentation model with both labeled and unlabeled images. Different from these methods, in this paper, we propose an MPL-based GAN to tackle the brain vessel image segmentation task. To this end, we present a novel MLP-GAN, which splits a 3D volumetric brain vessel image into three different dimensional 2D images and then feeds them into three different 2D cGANs to obtain the final segmentation. Meanwhile, the proposed MLP-GAN involves the recent MLP-Mixer into skip connections to mix token and channel information to learn global information to obtain better performance.

B. MLP-Mixer in Vision Models

MLP-Mixer [1] has been proved that simply multi-layered perceptrons (MLPs) can achieve high-quality vision results by two types of MLP layers: *channel-mixing* MLPs and *token-mixing* MLPs. The architecture of MLP-Mixers accepts a sequence of patches — a "$patches \times channels$" table, generated by rearrangement and linear projection. The channel-mixing MLPs build relationships among different channels by operating on every token independently. The token-mixing MLPs build relationships among different spatial locations with tokens by operating on every channel independently. Recently, the MLP-Mixer achieved state-of-the-art performance in vision tasks such as image generation [19], [20], image classification [21], [22], [23]. For instance, Res-MLP [21] proposed an affine transform layer so that it can achieve a deeper architecture and higher accuracy than the MLP-Mixer. gMLP [23] designed a spatial gating unit to increase the communications among spatial locations. It achieved a comparable accuracy of recognition compared with several state-of-the-art models. In this paper, we integrate the MLP-Mixer into our model to introduce cross-patch information.

III. The proposed MLP-GAN

A. Overview

The overview of our proposed MLP-GAN is illustrated in Figure 2. We first split the 3D volumetric image into a sequence of 2D plane images in terms of three dimensions (*i.e.,* coronal, sagittal, axial), respectively. Then, the sequence of 2D plane images is fed into the generator, which consists of three 2D networks with U-Net as the backbone. The generator outputs three 2D plane images with the same shape as the

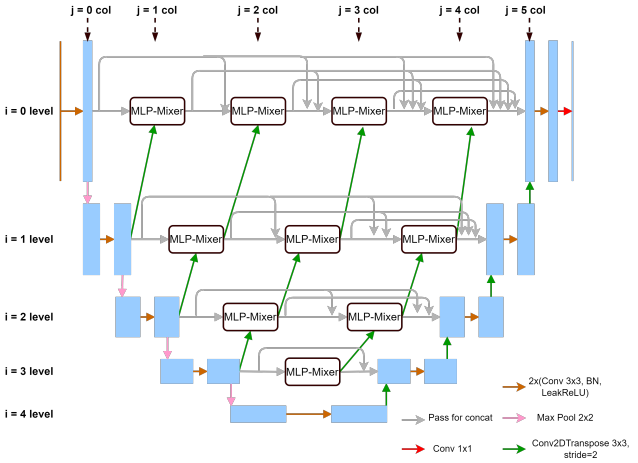

Fig. 3. The overview of one MLP-Mixer enhanced generator. Each generator utilizes a U-Net as the backbone. We redesign a pattern of skip connection with the integration of the MLP-Mixer block to obtain the ability to capture global information.

original input images. Next, these generated images are fed into the discriminator along with ground truth segmentation to discriminate whether they are true or false.

B. Memory-Friendly Isotropic 2D Input

Most 3D medical models require a 3D stack of images as input, which brings a large burden on hardware. Meanwhile, a medical image typically has a much high resolution. To solve this problem, we decompose the original 3D stack into three separate 2D plane images. For each iteration of training, we only feed three 2D orthogonal plane images into our network. In practice, the shape of our original brain vessel data and ground truth are (325, 304, 600). We crop the original data into several 3D volumetric images shaped (256, 256, 256). Then we split each 3D sample data into a sequence of 2D plane images by the same index on three different dimensions ranging [0, 255] to feed into three generators.

C. MLP-Mixer Enhanced Generator

The generator consists of three individual 2D U-Net-based networks, where each 2D network has identical layouts. Figure 3 illustrates a single 2D U-Net-based architecture. We redesign the patterns of skip connection in order to maximize their benefits. Each level in the decoder not only learns information from the previous level in the decoder but also learns information from the skip connection that consists of several MLP-Mixer blocks receiving information from the same level and the deeper level in the encoder. Then we concatenate these information to mix via *channel-mixing* and *token-mixing* MLPs to learn more semantic and overall information.

In the 2D U-Net-based generator, we integrate the MLP-Mixers into our generator as shown in Figure 3. We define that the U-Net has 5 levels. For i-th level, we define there are $(5-i)$ blocks. The function of each block can be expressed as the equation below,

$$\mathcal{H}^{i,j}(X) = \begin{cases} \mathrm{CNN}^{i,j}(X) & \text{if } j=0,\ i+j=5 \\ \mathrm{MLP}^{i,j}(X) & \text{otherwise,} \end{cases} \tag{1}$$

where i denotes the i-th layer, and j denotes j-th block in the same level, $\mathrm{CNN}(\cdot)$ denotes convolution layer function, and $\mathrm{MLP}(\cdot)$ denotes the MLP-Mixer function. More details for the MLP-Mixer function are shown at Section III-D MLP-Mixer block.

The function of the output of each block can be expressed as the following equation $\mathcal{O}^{i,j}(X) =$

$$\begin{cases} \mathcal{H}^{i,j}(\mathcal{I}) & if\ j=0 \\ \mathcal{H}^{i,j}(\mathcal{O}^{i,1}(X), \cdots, \mathcal{O}^{i,j-1}(X), \mathcal{O}^{i+1,j-1}(X)) & \text{otherwise,} \end{cases} \tag{2}$$

where $\mathcal{I}$ is the input images for the first block in each level. In this equation, when j=0, the block is the convolution layer, which only receives one input, called $\mathcal{I}$. The rest of the MLP-Mixers and CNNs will receive several inputs that contain all output of every left block $(\mathcal{O}^{i,0}(X), \cdots, \mathcal{O}^{i,j-1}(X))$ in the same level and the left one blocks in bottom one layer $(\mathcal{O}^{i+1,j-1}(X))$. All inputs will be concatenated and fed into the MLP-Mixer. In this way, since the pattern of skip connections can mix the spatial information between the current level and bottom level, which can pass more information to deeper layers, we can achieve better performance.

D. MLP-Mixer Block

Figure 4 illustrates the details of a modified MLP-Mixer block, which takes $X \in \mathbb{R}^{H \times W \times C}$ with a spatial resolution of $H \times W$ and C number of channels as an input. The MLP-Mixer firstly rearranges the original image to several non-overlapping patches and then perform a linear projection to get the shape "patches×channels". Specifically, the output of the rearrangement denotes $X_{reshape} \in \mathbb{R}^{(\frac{H}{S} \times \frac{W}{S}) \times (C \times S \times S)}$, where S denotes the size of patches. The "patches" and "channels" are equal to $\frac{H}{S} \times \frac{W}{S}$ and $C \times S \times S$, respectively.

In order to fit it in our network, we fix the number of neurons of the linear projection as the same as the last dimension of the shape after rearrangement, which can make the shape after rearrangement equalized to the shape after the linear projection. Specifically, the linear project denotes $W \in \mathbb{R}^{(C \times S \times S) \times (C \times S \times S)}$. The output of the linear project can be expressed as,

$$X_o = X_{reshape} W, X_o \in \mathbb{R}^{(\frac{H}{S} \times \frac{W}{S}) \times (C \times S \times S)} \tag{3}$$

After the linear projection, it connects two types MLPs with a LayerNormalization layer: token-MLP and channel-MLP, which mix token information and channel information, respectively. There is a matrix transpose between the token-MLP and the channel-MLP for the last two dimensions. For each MLP block, it comprises two fully-connected layers and a GELU activation in the middle. The MLP-Mixer block on $\mathrm{MLP}(\cdot)$ is as follows,

$$\begin{cases} U_{*,n} & = X_{*,n} + W_2 \sigma(W_1 \mathrm{LayerNorm}(X_o)_{*,n}) \\ \mathrm{MLP}_{m,*} & = X_{m,*} + W_4 \sigma(W_3 \mathrm{LayerNorm}(X_o)_{m,*}) \end{cases} \tag{4}$$

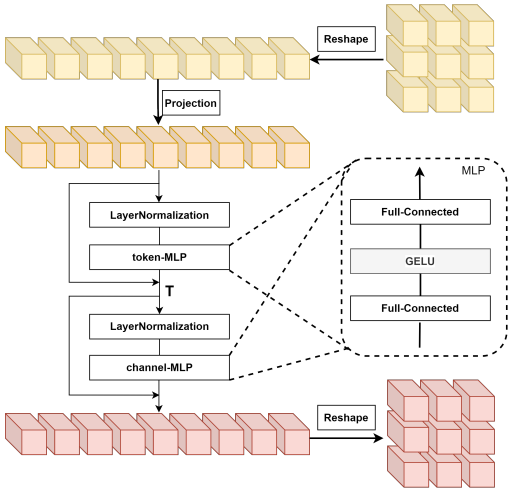

Fig. 4. The overview of MLP-Mixer block. The input feature map firstly is reshaped into several non-overlapping patches and then performs a linear projection. Next, it connects two types MLPs with a LayerNormalization layer: token-MLP and channel-MLP, which mix token information and channel information, respectively. Finally, the final output will be reshaped into the same shape as the input at the very beginning of the MLP-Mixer block.

where $n{=}1 \cdots C$, and $m{=}1 \cdots S$, σ is an element-wise non-linearity (GELU [24]). W_1 and W_2 denote two fully-connected layers in the token-MLP module. W_3 and W_4 denote two fully-connected layers in the channel-MLP module. The token-MLP module can capture token information that contains spatial information. The channel-MLP module has the ability to capture the channel information. Finally, the final output will be reshaped into the same shape as the input at the very beginning of the MLP-Mixer block.

E. Multi-Plane Discriminator

The discriminator also consists of three different 2D-base convolution layers' networks. Each 2D-based convolution layer's network takes generated images and ground truth as input. And then, their concatenation is fed into 4 times down-sample layers that consist of $2{\times}$(Conv2D 3×3, BN, LeakReLU). The shape of the output is $(B, 32, 32, 64)$, which can achieve the functionality of PatchGAN [7].

F. Overall Optimization Goal

The objective of our proposed MLP-GAN can be expressed as $\mathcal{L}^i_{cGAN} =$

$$\mathbb{E}_{x^i,y^i}[\log D(x^i, y^i)] + \mathbb{E}_{x^i,z}[1 - \log D(x^i, G(x^i, z))], \quad i = \text{sagittal, coronal, axial} \tag{5}$$

where G means the generator, trying to minimize this objective against an adversarial discriminator D which tries to maximize this objective. This objective consists of three parts which are for sagittal, coronal, and axial, respectively.

Meanwhile, we import the patch-wise balanced binary cross-entropy to endow the generator abilities near the ground truth output in a binary cross-entropy sense. We utilize $\mathcal{L}^i_{bBCE}$ as the extra loss function expressed:

$$-\frac{1}{N}\sum_{i=0}^{N} \beta(y^i_j \log(\hat{y^i_j}) + (1-\beta)(1-y^i_j)\log(1-\hat{y^i_j})), \quad i = \text{sagittal, coronal, axial} \tag{6}$$

where $\beta = |Y_-|/|Y|$ and $1-\beta = |Y_+|/|Y|$. $|Y_-|$ and $|Y_+|$ denote the mask and non-mask in ground truth sets, respectively. Because the number of mask pixels and non-mask pixels are extremely imbalanced. The balanced binary cross-entropy $\mathcal{L}^i_{bBCE}$ can balance the ratio of mask and non-mask. The loss function also consists of three parts that are for sagittal, coronal, and axial, respectively.

Our final objective function can be expressed as,

$$\mathcal{G} = \arg\min_G \max_D \frac{\sum_i \mathcal{L}^i_{cGAN}}{3} + \frac{\lambda \times \sum_i \mathcal{L}^i_{bBCE}}{3}, \quad i = \text{sagittal, coronal, axial} \tag{7}$$

where the final objective function consists of conditional GAN loss and balanced binary cross-entropy loss, where two losses average the effect of three different dimensions. Meanwhile, the λ coefficient is introduced to balance between $\mathcal{L}^i_{cGAN}$ and $\mathcal{L}^i_{bBCE}$.

IV. Experiments

A. Dataset

We use the public DeepVesselNet dataset [2] in our experiments. This dataset contains 136 images of brain vessels with shape $(325, 304, 600)$. The dataset is split into 96 training samples, 20 validation samples, and 20 test samples.

B. Evaluation Metrics

We employ the Dice coefficient and Intersection over Union (IoU) as our evaluation metrics to measure the performance of the generated images.

C. State-of-the-Art Comparisons

We compare our proposed approach with several leading convolutional-based methods (*i.e.*, 3D-UNet [25], VNet [26] and 2.5DNet [27]) and several GANs with different generators as the baseline models that include **i) 3D-U-Net-GAN:** utilizes an original 3D U-Net [25] as the generator, **ii) 3D-MLP-TransUNet-GAN [1]:** replaces the self-attention block in the TransUNet [28] with the MLP-Mixer for 3D version, **iii) 2.5D-U-Net-GAN:** utilizes three 2D U-Nets [27] for three different dimensional 2D images as the 2D generator, and **iv) 2.5D-MLP-TransUNet-GAN [1]:** 2.5D version of method ii). In this part, we crop the original data into several $(128, 128, 128)$ tensors as input.

Figure 5 illustrates the qualitative results of our method compared with other methods. As we can observe, the masks of the generated 2D plane images of the other methods are blurred, and there are some grey points in several masks. Meanwhile, the edges of some masks in generated 2D plane images have tiny trimmings. Compared to the other methods, our approach has better performance in the edges and masks.

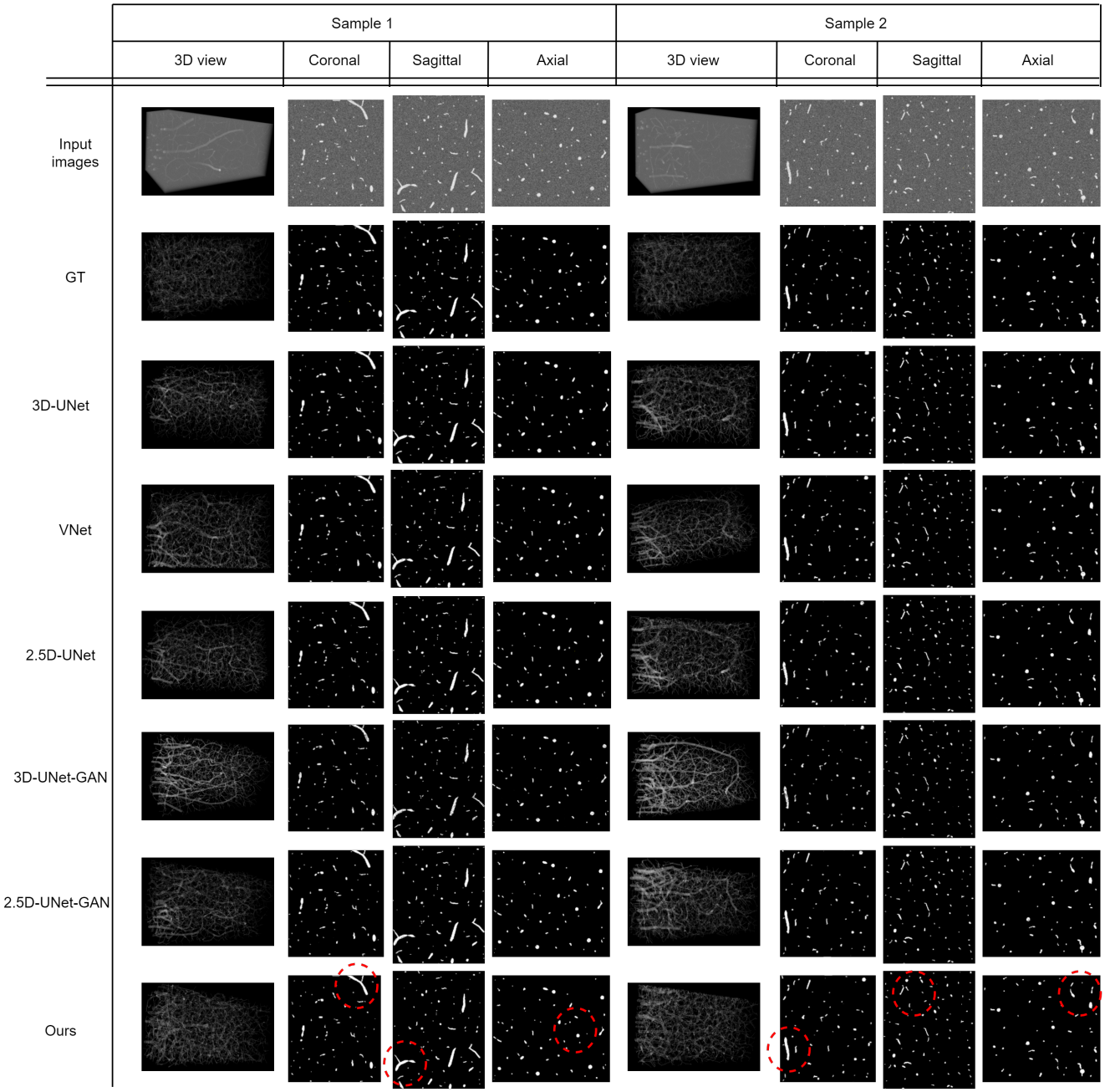

Fig. 5. The qualitative comparisons of our method and other state-of-the-art approaches, such as several leading convolutional-based methods(*i.e.*, 3D-UNet [25], VNet [26] and 2.5DNet [27]) and several GANs. We present two examples for 3D view and three different dimensional views (*i.e.*, sagittal, coronal, axial). As we can observe, the performance of our method is the best.

The quantitative comparison with state-of-the-art results is illustrated in Table I. For all metrics, higher means better. The number of Dice and IoU for our model is the highest, which demonstrates the performance of our model is the best. We can conclude that our proposed method achieves the best performance in all metrics, which validates the effectiveness of our proposed model. The results demonstrate our multi-view approach outperforms full 3D networks. In this way, we retain 3D spatial information and alleviate the memory issue compared to the 3D methods.

D. Ablation Study

In this section, we build several variants of 2D generators based on the 2.5D-UNet-GAN architecture as our baselines (*i.e.*, S1, S2, S3) as shown in Table II. All architectures follow the rule that there are three 2D U-Net-based generators to compose a whole generator. The discriminator also consists of the same three networks built by 2D convolution layers. The difference among these baselines is only about 2D U-Net-based generators. We only modify the skip connections of 2D generators. i) S1 is the original 2D UNet with skip

TABLE I
STATE-OF-THE-ART COMPARISONS.

Method	Dice ↑	IoU ↑
3D-UNet [25]	0.894	0.946
VNet [26]	0.921	0.958
2.5D-UNet [27]	0.891	0.935
3D-UNet-GAN [25]	0.861	0.927
3D-MLP-TransUnet-GAN [28]	0.981	0.964
2.5D-UNet-GAN [27]	0.986	0.971
2.5D-MLP-TransUnet-GAN [28]	0.982	0.965
MLP-GAN (Ours)	**0.992**	**0.979**

TABLE II
THE ABLATION STUDIES OF 2D GENERATOR.

Method	Dice ↑	IoU ↑
S1 UNet	0.986	0.971
S2 UNet+MLP w/o same and lower level	0.988	0.976
S3 UNet+MLP w same and w/o lower level	0.989	0.979
MLP-GAN (Ours)	**0.992**	**0.979**

connections. ii) S2 replaces the skip connections with the MLP-Mixer layers. For the i-th level, the number of MLP-Mixer layers is equal to $4-i$. iii) S3 involves skip connections, so each MLP-Mixer layer receives all output from the previous MLP-Mixer layers at the same level.

The comparison results are illustrated in Table II. S2 replaces the skip connections with the MLP-Mixer layers and achieves a better performance than S1, which demonstrates the effectiveness of the MLP-Mixer layers as the components for the skip connections. In this way, our model has the ability to capture global information. Compared to S2 and S3, our model involves information from both the same level and lower levels and achieves the best results, which can validate the effectiveness of our model. Our model can learn different levels of information in this way.

E. Training and Integration Details

We run all experiments based on Python 3.9, PyTorch 1.11.0 and Ubuntu 18.04. All models were trained using a single NVIDIA RTX A5000. We utilize Adam as our optimizer and set the learning rate to 2e-4. We set the maximum epochs to 1000. To train our MLP-GAN stably, each block in the encoder and decoder consists of a Convolutional layer, Batch Normalization and Leaky ReLU activation.

For fair comparisons among all different methods, the number of channels for all layers in the same location is the same whatever the model is 2D or 3D based. For example, the number of channels of the first hidden layer in the generator is 8. The deeper one is 16. In the experiments, the shape of the input tensor for 3D models is $(128, 128, 128, 1)$ whereas the 2D models' input shape is $(256, 256, 1)$.

We firstly create an empty matrix of the same size as 3D input images. Because we split each 3D input image into several $(256, 256, 256, 1)$ patches, we need to recover the same number of patches. And then we slice the several $(256, 256, 256, 1)$ patches into $256\times(256, 256, 1)$ in terms of three dimensions (*i.e.,* coronal, sagittal, axial) by the same index range [0, 255], which means we have $3\times256\times(256, 256, 1)$ 2D images. Next, we feed all images into our networks to train. As for integration, the generator will predict the same number and size of 2D images. We follow the same way that split by the same index to recover each $(256, 256, 256, 1)$ 3D patches. Finally, we use the several 3D patches to recover the final images of the same size as the original input images.

TABLE III
COMPARISONS WITH FLOPS AND PARAMETERS. (M: MILLION, G: GFLOPS).

Method	FLOPs↓	Params↓
3D-UNet [25]	61.83G	3.40M
2.5D-UNet [27]	1.44G	3.40M
3D-UNet-GAN [25]	80.43G	3.62M
3D-MLP-TransUnet-GAN [28]	84.90G	420.68M
2.5D-UNet-GAN [27]	1.77G	3.62M
2.5D-MLP-TransUnet-GAN [28]	1.93G	28.48M
MLP-GAN (Ours)	23.23G	46.22M

F. Comparisons with Time and Memory

We compared several methods in terms of time and memory using FLOPs and the number of parameters as shown in Table III. Our method decomposes 3D volumetric images into a sequence of 2D plane images. In this way, the FLOPs of our method decrease significantly, and the number of parameters increases a little compared with 3D U-Net. The reason about the number of parameters of our model is higher than the 2.5D-UNet-GAN is the introduction of MLP-Mixer layers. The introduction of the MLP-Mixer as the component of redesigned skip connections will bring significant improvement in terms of accuracy. It is feasible for our model to bring about a reasonable number of parameters along with a significant improvement.

V. CONCLUSIONS

In this paper, we propose a novel multi-viewed MLP-GAN that decomposes 3D volumetric images into a sequence of 2D plane images in terms of three dimensions(*i.e.,* coronal, sagittal, axial), respectively. And then feed the sequence of 2D plane images into three different 2D U-Net-based networks as our generator, which not only decreases the complexity and cost but also retains the spatial information. In each 2D generator, we introduce a redesigned pattern of skip connection with the integration of the MLP-Mixer block to obtain the ability to capture global information. In this way, each layer in the decoder can learn more semantic information since MLP-Mixer blocks can mix deeper level layers and current level layer information from the encoder to learn overall information, which can maximize the benefits of skip connections. The experimental results demonstrate that our method outperforms the state-of-the-art approaches.

Acknowledgments: Y.Y. and D.C. received support by National Institutes of Health (NIH) 1RF1MH124611, 1RF1MH123402. D.C. also received support by National Science Foundation NeuroNex-1707316.

REFERENCES

[1] I. Tolstikhin, N. Houlsby, A. Kolesnikov, L. Beyer, X. Zhai, T. Unterthiner, J. Yung, D. Keysers, J. Uszkoreit, M. Lucic *et al.*, "Mlp-mixer: An all-mlp architecture for vision," *arXiv:2105.01601*, 2021.

[2] G. Tetteh, V. Efremov, N. D. Forkert, M. Schneider, J. Kirschke, B. Weber, C. Zimmer, M. Piraud, and B. H. Menze, "Deepvesselnet: Vessel segmentation, centerline prediction, and bifurcation detection in 3-d angiographic volumes," *Frontiers in Neuroscience*, vol. 14, 2020.

[3] O. Ronneberger, P. Fischer, and T. Brox, "U-net: Convolutional networks for biomedical image segmentation," in *MICCAI*, 2015.

[4] Z. Akkus, A. Galimzianova, A. Hoogi, D. L. Rubin, and B. J. Erickson, "Deep learning for brain mri segmentation: state of the art and future directions," *Journal of digital imaging*, vol. 30, no. 4, pp. 449–459, 2017.

[5] M. Avendi, A. Kheradvar, and H. Jafarkhani, "A combined deep-learning and deformable-model approach to fully automatic segmentation of the left ventricle in cardiac mri," *Medical image analysis*, vol. 30, pp. 108–119, 2016.

[6] I. Goodfellow, J. Pouget-Abadie, M. Mirza, B. Xu, D. Warde-Farley, S. Ozair, A. Courville, and Y. Bengio, "Generative adversarial nets," in *NeurIPS*, 2014.

[7] P. Isola, J.-Y. Zhu, T. Zhou, and A. A. Efros, "Image-to-image translation with conditional adversarial networks," in *CVPR*, 2017.

[8] H. Tang, D. Xu, N. Sebe, Y. Wang, J. J. Corso, and Y. Yan, "Multi-channel attention selection gan with cascaded semantic guidance for cross-view image translation," in *CVPR*, 2019.

[9] M. Mirza and S. Osindero, "Conditional generative adversarial nets," *arXiv:1411.1784*, 2014.

[10] T. Karras, S. Laine, and T. Aila, "A style-based generator architecture for generative adversarial networks," in *CVPR*, 2019.

[11] Y. Xue, T. Xu, H. Zhang, L. R. Long, and X. Huang, "Segan: Adversarial network with multi-scale l 1 loss for medical image segmentation," *Neuroinformatics*, vol. 16, no. 3, pp. 383–392, 2018.

[12] P. Moeskops, M. Veta, M. W. Lafarge, K. A. Eppenhof, and J. P. Pluim, "Adversarial training and dilated convolutions for brain mri segmentation," in *Deep learning in medical image analysis and multimodal learning for clinical decision support*. Springer, 2017, pp. 56–64.

[13] J. Son, S. J. Park, and K.-H. Jung, "Retinal vessel segmentation in fundoscopic images with generative adversarial networks," *arXiv:1706.09318*, 2017.

[14] D. Yang, D. Xu, S. K. Zhou, B. Georgescu, M. Chen, S. Grbic, D. Metaxas, and D. Comaniciu, "Automatic liver segmentation using an adversarial image-to-image network," in *MICCAI*, 2017.

[15] Y. Zhang, L. Yang, J. Chen, M. Fredericksen, D. P. Hughes, and D. Z. Chen, "Deep adversarial networks for biomedical image segmentation utilizing unannotated images," in *MICCAI*, 2017.

[16] W. Dai, N. Dong, Z. Wang, X. Liang, H. Zhang, and E. P. Xing, "Scan: Structure correcting adversarial network for organ segmentation in chest x-rays," in *Deep learning in medical image analysis and multimodal learning for clinical decision support*, 2018, pp. 263–273.

[17] W. Zhu, X. Xiang, T. D. Tran, G. D. Hager, and X. Xie, "Adversarial deep structured nets for mass segmentation from mammograms," in *ISBI*, 2018.

[18] A. K. Mondal, J. Dolz, and C. Desrosiers, "Few-shot 3d multi-modal medical image segmentation using generative adversarial learning," *arXiv:1810.12241*, 2018.

[19] G. Cazenavette and M. L. De Guevara, "Mixergan: An mlp-based architecture for unpaired image-to-image translation," *arXiv:2105.14110*, 2021.

[20] B. Ren, H. Tang, and N. Sebe, "Cascaded cross mlp-mixer gans for cross-view image translation," in *BMVC*, 2021.

[21] H. Touvron, P. Bojanowski, M. Caron, M. Cord, A. El-Nouby, E. Grave, A. Joulin, G. Synnaeve, J. Verbeek, and H. Jégou, "Resmlp: Feedforward networks for image classification with data-efficient training," *arXiv:2105.03404*, 2021.

[22] T. Yu, X. Li, Y. Cai, M. Sun, and P. Li, "S ^{2}-mlp: Spatial-shift mlp architecture for vision," *arXiv:2106.07477*, 2021.

[23] H. Liu, Z. Dai, D. R. So, and Q. V. Le, "Pay attention to mlps," *arXiv:2105.08050*, 2021.

[24] D. Hendrycks and K. Gimpel, "Gaussian error linear units (gelus)," *arXiv:1606.08415*, 2016.

[25] Ö. Çiçek, A. Abdulkadir, S. S. Lienkamp, T. Brox, and O. Ronneberger, "3d u-net: learning dense volumetric segmentation from sparse annotation," in *MICCAI*, 2016.

[26] F. Milletari, N. Navab, and S.-A. Ahmadi, "V-net: Fully convolutional neural networks for volumetric medical image segmentation," in *2016 fourth international conference on 3D vision (3DV)*. IEEE, 2016, pp. 565–571.

[27] C. Angermann, M. Haltmeier, R. Steiger, S. Pereverzyev, and E. Gizewski, "Projection-based 2.5 d u-net architecture for fast volumetric segmentation," in *2019 13th International conference on Sampling Theory and Applications (SampTA)*. IEEE, 2019, pp. 1–5.

[28] J. Chen, Y. Lu, Q. Yu, X. Luo, E. Adeli, Y. Wang, L. Lu, A. L. Yuille, and Y. Zhou, "Transunet: Transformers make strong encoders for medical image segmentation," *arXiv:2102.04306*, 2021.